Euro. Jnl of Applied Mathematics (2003), *vol.* 14, *pp.* 15–38. © 2003 Cambridge University Press
DOI: 10.1017/S0956792502005089 Printed in the United Kingdom

Identification of nonlinear B–H curves based on magnetic field computations and multigrid methods for ill-posed problems

BARBARA KALTENBACHER[1], MANFRED KALTENBACHER[2] and STEFAN REITZINGER[3]

[1] *Industrial Mathematics Institute, University of Linz, A-4040 Linz, Austria*
[2] *Department of Sensor Technology, University of Erlangen, D-91056 Erlangen, Germany*
[3] *SFB013 Numerical and Symbolic Scientific Computing, University of Linz, A-4040 Linz, Austria*

(*Received 1 May 2001; revised 20 February 2002*)

Our task is the identification of the reluctivity $\nu = \nu(B)$ in $\mathbf{H} = \nu(B)\mathbf{B}$, $(B = |\mathbf{B}|)$ from measurements of the magnetic flux for different excitation currents in a driving coil, in the context of a nonuniform magnetic field distribution. This is a nonlinear inverse problem and ill-posed in the sense of unstable data dependence, whose solution is done numerically by a Newton type iterative scheme, regularized by an appropriate stopping criterion. The computational complexity of this method is determined by the number of necessary forward evaluations, i.e. the number of numerical solutions to the three-dimensional magnetic field problem. We keep the effort minimal by applying a special discretization strategy to the inverse problem, based on multigrid methods for ill-posed problems. Numerical results demonstrate the efficiency of the proposed method.

1 Introduction

In many practical applications of electromagnetism, the relation between the magnetic field strength $\mathbf{H}$ and the magnetic flux density $\mathbf{B}$ is nonlinear, i.e. the magnetic permeability μ or its reciprocal, the reluctivity ν, in

$$\begin{aligned} \mathbf{B} &= \mu(H)\mathbf{H} \\ \mathbf{H} &= \nu(B)\mathbf{B} \end{aligned} \tag{1.1}$$

where $H = |\mathbf{H}|$, $B = |\mathbf{B}|$ are not constant. This happens especially in the case of large excitations, as they occur, for example, in magneto-mechanical actuators. A typical B–H curve is approximately linear only in the range of relatively low magnetic flux density, but with increasing H changes to a nonlinear behaviour to finally become saturated as H gets large; see Figure 1 for an example.

To be able to do reliable numerical magnetic field simulations, it is crucial to know the shape of this curve precisely. So far, this has been obtained via special experimental setup – the so-called Epstein apparatus – using very thin samples of the material under investigation, arranged in an appropriate pattern, to achieve a uniform distribution of the magnetic flux density. Namely, if B is constant over the whole test sample, then the

https://doi.org/10.1017/S0956792502005089 Published online by Cambridge University Press

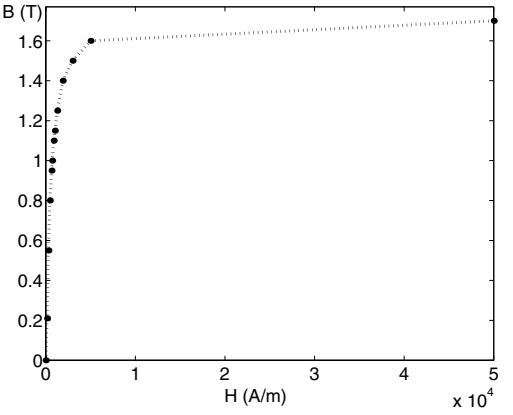


FIGURE 1. Typical B–H-curve shape.

relations

$$B = \frac{n_w}{A_t}\Phi, \quad H = \frac{n_w}{l_t}I, \tag{1.2}$$

hold, where n_w is the number of coil windings, A_t a typical cross-sectional area of the test sample, and l_t a typical length of the magnetic flux lines in the experimental setup. These allow an explicit computation of the ratio ν between H and B from measured data of the magnetic flux $\Phi = \Phi(I)$ corresponding to different values of the imposed current I, that yield a collection of points on the desired curve $\nu = \nu(B)$.

This measurement setup is, however, often hard or impossible to realize (cf. e.g. Ioan *et al.* [9]), or yields too inexact approximations of the curve. We therefore propose to replace the combination of 'complicated measurement setup with simple mathematics' by a combination of 'simple measurement setup with more sophisticated mathematical methods' of extracting the parameter information from the given data. More precisely, we use an inversion scheme that is based on full three-dimensional simulations of the magnetic field problem, and are therefore able to encounter for variations of the magnetic flux density over the region covered by the probe and its surroundings.

The concrete mathematical model we deal with is given by free, as well as the constitutive relationship for Maxwell's equations (e.g. c.f. Ida & Bastos [8]) in the steady state case for isotropic media which results in

$$\begin{aligned} \nabla \times (\nu(B)\nabla \times \mathbf{A}) &= \mathbf{J} \quad \text{in } D \\ \mathbf{n} \times \mathbf{A} &= 0 \quad \text{on } \Gamma_B \end{aligned} \tag{1.3}$$

where

$$\mathbf{J} = \begin{cases} \dfrac{I}{|\Omega_c|}\mathbf{e}_J & \text{in } D_c \\ 0 & \text{else} \end{cases}$$

is the imposed current density,

$$\Phi = \oint_c \mathbf{A} \cdot \mathbf{ds} = \int_{\Omega_c} \mathbf{B} \cdot \mathbf{n}\, d\sigma$$

https://doi.org/10.1017/S0956792502005089 Published online by Cambridge University Press

is the magnetic flux

$$\mathbf{B} = \nabla \times \mathbf{A}, \quad B = |\mathbf{B}|,$$

$\mathbf{A}$ is the magnetic vector potential, $\mathbf{e}_J$ the unit vector in current direction, D_c the region covered by the excitation coil, Ω_c its cross sectional area, and the equality of the integral $\oint_c$ of $\mathbf{A}$ along the coil winding with the integral over Ω_c of $\mathbf{B}$ holds due to Stokes' theorem.

We have to identify the nonlinear real function $\nu = \nu(B)$ from measurements of the magnetic flux Φ for different currents I in an excitation coil, i.e. the data also consists of (in reality discrete measurements of) a scalar function $\Phi = \Phi(I)$ of one variable. This is a nonlinear inverse problem and ill-posed as will be pointed out below. Consequently small perturbations in the data (which naturally occur due to measurement noise), can lead to large deviations in the solution, which can obviously cause serious problems in a naive numerical approach. We therefore have to implement some appropriate numerical approximation scheme, i.e. a so-called regularization method [3, 5, 16, 17, 18, 19, 20]) for its stable solution. This is here done by a Newton-type method with iterative solution of the linearized equations, where both the outer and the inner iteration are stopped at an a posteriori chosen appropriate index to prevent the increasingly propagated data noise from destroying the approximation.

The main challenge in this approach lies in the fact that the corresponding forward problem, which repeatedly appears in the course of the inversion procedure, demands high computational effort. For each value of I, the large scale nonlinear three-dimensional magnetic field equation (1.3) has to be solved. Even if, as done here, by methods that are known to be very efficient, and the accuracy for the nonlinear solution is chosen adaptively according to the state of convergence in the inversion iteration, there is still a need to take care of efficiency by means of an improved inversion procedure. At this point the usefulness of multilevel methods for this inverse problem becomes clear. By an adaptive choice of the discretization in data space, using appropriate multigrid operators for ill-posed problems, we can minimize the number of necessary boundary value problem (1.3) solutions and thereby significantly decrease the overall computational effort for the parameter identification.

The paper is organized as follows. The inversion issue in § 2 forms the main emphasis of this paper and is divided into three subsections: After formulating the inverse problem in § 2.1 we motivate the use of multigrid methods in § 2.2, by proposing either to combine a Newton type method with a full multigrid method as a linear solver (i.e. iterative regularization by coarse discretization), or to use directly a nonlinear full multigrid method. § 2.3 contains the necessary results on some multigrid methods for ill-posed problems. In § 3 we describe some important realization aspects, namely measurement setup, numerical solution of the forward problem, and curve approximation. § 4 shows numerical tests verifying the performance of multigrid methods for the ill-posed equations relevant for the identification problem under consideration and provides numerical examples of our B–H curve reconstruction technique. The final § 5 gives an outlook, containing especially the applicability of our approach to other parameter identification problems.

In the following we will use the notation c or C for positive constants that are typically 'small' or 'large', respectively. They may have different values whenever they appear in the text.

https://doi.org/10.1017/S0956792502005089 Published online by Cambridge University Press

2 The inverse problem of B–H curve identification

2.1 Formulation as a nonlinear operator equation

We denote by F the forward operator, i.e. the application of the measurement operator (mapping a magnetic vector potential to the corresponding magnetic flux through the coil) to the parameter-to solution map for (1.3), i.e.

$$\begin{aligned} F : \mathscr{D}(F) \subseteq X &\to Y \\ \nu &\mapsto \left(\oint_c \mathbf{A}^I \cdot \mathbf{ds} \right)_{I \in [\underline{I}, \overline{I}]} \end{aligned}$$

where, for all $I \in [\underline{I}, \overline{I}]$, $\mathbf{A}^I$ solves

$$\int_D \nabla \times \mathbf{A}' \cdot \nu(|\nabla \times \mathbf{A}^I|)\, \nabla \times \mathbf{A}^I \, dV = I \frac{1}{|\Omega_c|} \int_{D_c} \mathbf{A}' \cdot \mathbf{e}_J \, dV \quad \forall \mathbf{A}' \in H_0(curl), \tag{2.1}$$

i.e. the weak formulation of (1.3), with

$$H_0(curl) := \{\mathbf{A} \in L^2(D) \ : \ \nabla \times \mathbf{A} \in L^2(D) \ \wedge \ \mathbf{n} \times \mathbf{A} = 0 \text{ on } \Gamma_B\},$$

where X and Y are appropriate function spaces to be defined below, and $\mathscr{D}(F) \subseteq X$ is such that $F : \mathscr{D}(F) \to Y$ is well-defined.

Well-posedness of the forward problem is essential not only in the context of our identification problem. Our final aim is of course to employ the reconstructed reluctivity ν in simulations of general application problems beyond our experimental setup, so problems of the form (1.3) with general $\mathbf{J}$ and D should be well-posed.

To achieve this, we have to guarantee solvability of (2.1) via the calculus of variations and the fact that a solution $\mathbf{A}^I$ to (2.1) minimizes the functional

$$\mathbf{A} \mapsto \int_D \left(\int_0^{|\nabla \times \mathbf{A}|} H(B)\, dB - \mathbf{A} \cdot \mathbf{J} \right) dV. \tag{2.2}$$

(Note that due to the nontrivial nullspace of the curl operator, we would have to impose an additional criterion like $\operatorname{div} \mathbf{A}^I = 0$ to guarantee uniqueness of $\mathbf{A}^I$ itself; however, we evaluate a quantity derived from $\mathbf{B}^I = \nabla \times A^I$, which is in its turn unique, also without such a kind of gauge.) For this purpose we need convexity of the functional defined in (2.2) and hence strict monotonicity of the H–B curve – a physically natural requirement, which in our numerical computations has to be explicitly maintained by imposing uniform bounds on the first derivative of the function $B \mapsto H(B) = \nu(B)B$, more precisely by bounding ν'. Moreover, there will be a need to evaluate ν' whenever we want to solve general nonlinear Boundary Value Problems (BVPs) of the form (1.3) by a Newton type method. Therefore, our domain $\mathscr{D}(F)$ in the parameter space X has to be a subset of a space containing W^1_∞ (the space of a.e. uniformly bounded functions with a.e. uniformly bounded weak first derivative). To work with an inner product space we choose a Sobolev space of order larger than $3/2$:

$$\mathscr{D}(F) := \left\{ \tilde{\nu} \in H^2([\underline{B}, \overline{B}]) \mid \|\tilde{\nu} - \nu_0\|_{W^1_\infty} \leqslant \rho \right\}, \quad X = H^2([\underline{B}, \overline{B}]),$$

where ν_0 is an initial guess that is supposed to be sufficiently close to the sought for exact

https://doi.org/10.1017/S0956792502005089 Published online by Cambridge University Press

v, and $\rho > 0$ is a small radius such that, on the one hand $\mathscr{D}(F)$ contains v, and on the other hand $B \mapsto \tilde{\nu}(B)B$ is strictly monotone for all $\tilde{\nu} \in \mathscr{D}(F)$. The interval $[\underline{B}, \overline{B}]$ on which we expect to be able to identify ν depends on the measurement interval $[\underline{I}, \overline{I}]$. Motivated by the formulas (1.2) (which are valid for the special case of a uniformly distributed magnetic field) we set

$$[\underline{B}, \overline{B}] := \left[\frac{n_w}{A_t}\Phi(\underline{I}), \frac{n_w}{A_t}\Phi(\overline{I})\right],$$

which will (also in the non-uniform situation) contain all B-values of interest, as long as we use a sufficiently wide measurement interval $[\underline{I}, \overline{I}]$ covering the region of saturation, where the reluctivity does not change any more.

We mention that both the measurement in practice and the computational evaluation of the measurement operator

$$\mathbf{A} \mapsto \oint_c \mathbf{A} \cdot \mathbf{ds} = \int_{\Omega_c} \mathbf{B} \cdot \mathbf{n}\, d\sigma,$$

are in fact done by averaging over the coil, i.e. instead of evaluating surface integrals of $\mathbf{B}$ over Ω_c, the volume integral over the whole cylinder formed by the coil, normed by the coil height h (and possibly multiplied by a filling factor in $(0, 1)$ representing the density of the windings within the coil) is regarded as the measured quantity:

$$\frac{1}{h}\int_{\Omega_c \times [0,h]} B_n \, dV \tag{2.3}$$

with B_n the component of B in $\mathbf{n}$ direction, i.e. parallel to the coil axis. The quantity in (2.3) is bounded by the $L^2(D)$-norm of $\mathbf{B}$ and hence well-defined for $\mathbf{A} \in H_0(curl)$.

Due to the fact that only values but not higher-order derivatives of Φ can be measured, and since we want to work in Hilbert spaces, the data space is naturally

$$Y = L^2([\underline{I}, \overline{I}]).$$

By means of the forward operator F we can formulate our inverse problem as a nonlinear operator equation

$$F(\nu) = \Phi, \tag{2.4}$$

which is ill-posed as can be seen from the special case of a uniformly distributed magnetic field. In this case, relation (1.2) is valid and we see that a reconstruction in $X = H^2([\underline{B}, \overline{B}])$ of the function

$$B \mapsto \nu(B) = \frac{H(B)}{B} = \frac{n_w}{l_t}\frac{\Phi^{-1}\left(\frac{A_t}{n_w}B\right)}{B} \tag{2.5}$$

from L^2 measurements of Φ is about as ill-posed as twice differentiation – for a more precise quantification of the ill-posedness of the parameter identification problem, see Lemma 1. Note that by (2.5) we would expect well-posedness if we could choose the same order of smoothness for the parameter and for the measurement space, which, however, would not make sense, as the argument for our choice of the spaces X and Y shows.

https://doi.org/10.1017/S0956792502005089 Published online by Cambridge University Press

Due to this ill-posedness and since the measurements will typically be contaminated with noise of some noise level $\delta > 0$, i.e. we have Φ^δ with

$$\|\Phi - \Phi^\delta\|_Y \leqslant \delta, \tag{2.6}$$

we must regularize (2.4) [3, 5, 16, 17, 18, 19, 20]. Some typical regularizing principles for general ill-posed operator equations

$$F(v) = \Phi \tag{2.7}$$

with noisy data Φ^δ satisfying (2.6) are:

(1) Tikhonov method: $\|F(v_\alpha) - \Phi^\delta\|_Y^2 + \alpha\|v_\alpha\|_X^2$, $\alpha > 0$; regularization by *spectrum shift*.
(2) Iterative solution: $v_n = \psi(v_{n-1}, \Phi^\delta)$; regularization by *early stopping*.
(3) Projection onto a finite-dimensional space $Y_l \subset Y$: $Q^l F(v^l) = Q^l \Phi^\delta$; regularization by *coarse discretization*.

Here, the first of these three items is quoted due to the fact that it is still certainly the most well-known one. The second and third ones are listed, since they are closely related to the regularization we are going to apply to our parameter identification problem (and its linearization). A crucial point is the correct choice of the regularization parameter α, or, in our situation, of the stopping index n or discretization level l, to achieve an optimal trade-off between approximation and stability. A well-known and effective optimal a posteriori strategy for this purpose is Morozov's discrepancy principle (cf. e.g. [3], [17]), where out of a family (parameterized by α or n or l) of regularized approximations the most stable one is chosen, under the restriction that the residual is of the order of magnitude of the noise level (see (2.10) below).

2.2 Motivation of multigrid methods for the inverse problem

The iterative solution of (2.4) by an (inexact) Newton type method

$$v_{k+1} = v_k + s_k \text{ where } F'(v_k)[s_k] \approx \Phi - F(v_k)$$

involves the (approximate) solution of the linear operator equation

$$T_k s = b_k \tag{2.8}$$

with

$$\begin{aligned} T_k : X &\to Y, \\ s &\mapsto \left(\oint_c \mathbf{S}^I \cdot \mathbf{ds} \right)_{I \in [\underline{I}, \overline{I}]}, \end{aligned}$$

where for all $I \in [\underline{I}, \overline{I}]$, $\mathbf{S}^I$ solves

$$\int_D \nabla \times \mathbf{A}' \cdot \left(v_k\left(B_k^I\right) + v_k'\left(B_k^I\right) B_k^I \, proj_{\mathbf{e}_{B_k^I}} \right) (\nabla \times \mathbf{S}^I) \, dV = -\int_D \nabla \times \mathbf{A}' \cdot s\left(B_k^I\right) B_k^I \, dV, \tag{2.9}$$

$$b_k(I) := \Phi(I) - \oint_c \mathbf{A}_k^I \cdot \mathbf{ds}, \quad I \in [\underline{I}, \overline{I}],$$

https://doi.org/10.1017/S0956792502005089 Published online by Cambridge University Press

where

$$\mathbf{B}_k^I = \nabla \times \mathbf{A}_k^I, \quad B_k^I = \left|\mathbf{B}_k^I\right|, \quad \mathbf{e}_{B_k^I} = \frac{1}{B_k^I}\mathbf{B}_k^I, \quad proj_{\mathbf{e}_{B_k^I}} := \mathbf{e}_{B_k^I}\mathbf{e}_{B_k^I}^T,$$

and $\mathbf{A}_k^I$ solves (2.1) with $\nu := \nu_k$.

To account for the ill-posedness of the nonlinear problem (2.4), we regularize the Newton iteration by stopping it according to a discrepancy principle as described above, i.e. at

$$k = \min \text{ s.t. } \|F(\nu_k) - \Phi^\delta\|_Y \leqslant \tau\delta \tag{2.10}$$

with some *a priori* chosen constant $\tau > 1$.

It has to be noticed that the linear problems (2.8) in each Newton step are also ill-posed. Roughly speaking, the linear operator T_k acts like the inverse of a differential operator, which implies that, like in the underlying nonlinear equation, a solution to (2.8) in general does not depend continuously upon the data Φ. A quantification of this ill-posedness in a form in which we will need it for constructing appropriate multigrid operators, can be given in terms of the smoothing property of the adjoint T_k^*, which, as can be easily checked, is for any $z \in Y = L^2([\underline{I},\overline{I}])$, given by

$$(T_k^* z)(\lambda) = \int_{[\underline{I},\overline{I}]} z(I) \int_D \eta\left(\lambda - B_k^I\right)\mathbf{B}_k^I \cdot (\nabla \times \mathbf{Z}^I)\, dV\, dI, \tag{2.11}$$

where

$$(\mathscr{F}\eta)(\xi) = \frac{1}{(1+\xi^2)^2}(\mathscr{F}\delta_0)(\xi),$$

with $\mathscr{F}$ denoting the Fourier transform and δ_0 the Dirac delta distribution (not to be confused with the noise level δ) i.e.

$$\eta(\lambda) = \frac{1}{2}\sqrt{\frac{\pi}{2}}(1+|\lambda|)\exp(-|\lambda|),$$

and $\mathbf{Z}^I$ solves

$$\int_D \nabla \times \mathbf{A}' \cdot \left(\nu_k\left(B_k^I\right)\, id \; + \nu_k'\left(B_k^I\right)B_k^I \; proj_{\mathbf{e}_{B_k^I}}\right)(\nabla \times \mathbf{Z}^I)\, dV = \oint_c \mathbf{A}' \cdot \mathbf{ds}.$$

Proposition 1 *Under the conditions* $I \to \mathbf{B}_k^I \in W_\infty^1(\underline{I},\overline{I}; L^\infty(D)) \cap H^2(\underline{I},\overline{I}; L^2(D))$, $I \to \mathbf{Z}^I \in H^2(\underline{I},\overline{I}; H_0(curl))$, *the operator* T_k^* *can be extended to a continuous linear operator from* $(H^\sigma([\underline{I},\overline{I}]))^*$ *to* $H^2([\underline{B},\overline{B}])$ *for any* $\sigma \in (0, \frac{3}{2})$.

(Here $W_p^s(\underline{I},\overline{I}; X)$ denotes the usual Sobolev space of functions on the interval $[\underline{I},\overline{I}]$ with values in the Banach space X.)

Proof see the Appendix. □

Proposition 1 states that T_k^* is smoothing 'of order'

$$p = \frac{3}{2},$$

https://doi.org/10.1017/S0956792502005089 Published online by Cambridge University Press

and by

$$\|T_k s\|_{H^\sigma([\underline{L},\overline{L}])} = \sup_{z\in Y} \frac{\langle T_k s, z\rangle_{L^2([\underline{L},\overline{L}])}}{\|z\|_{(H^\sigma([\underline{L},\overline{L}]))^*}} = \sup_{z\in Y} \frac{\langle s, T_k^* z\rangle_X}{\|z\|_{(H^\sigma([\underline{L},\overline{L}]))^*}}$$

$$\leqslant \|T_k^*\|_{(H^\sigma([\underline{L},\overline{L}]))^*\to H^2([\underline{B},\overline{B}])} \|s\|_X$$

for any $s \in X$, $\sigma \in (0, \frac{3}{2})$, implies that the range $T_k X$ of T_k is non-closed in Y, and hence (2.8) is ill-posed, so that regularization is also necessary for the linearized problems.

On the other hand, note that to formulate (2.8), for each value of I a linear magnetic field problem (2.9) for setting up the system matrix, and a nonlinear one (2.1) for computing the right-hand side, has to be solved. Therefore, it is desirable to keep the dimension of the discretized measurement space (i.e. the number of different $I - \Phi$ pairs entering into the computations) as low as possible – subject to approximation requirements as usual in an inexact Newton method (namely such that the linear residual is by some factor $\eta_k \in (0,1)$ smaller than the nonlinear residual in the actual Newton step, see (2.14) below). This just corresponds to regularization by coarse discretization, with the refinement level chosen by a discrepancy principle [10].

More precisely, consider the projection of (2.8) onto a space Y_l out of a sequence $(Y_l)_{l=1,2,3,\ldots}$ of nested finite dimensional subspaces of Y, whose union is dense in Y:

$$Y_1 \subseteq Y_2 \subseteq Y_3 \ldots \subseteq Y, \quad \overline{\bigcup_l Y_l} = Y.$$

In our concrete parameter identification problem, the spaces Y_l consist of piecewise linear splines on a not necessarily equidistant partition of the interval $[\underline{B}, \overline{B}]$, where the successive refinement is done by bisection of the partition intervals. Choosing out of the (infinitely many) solutions to the projected equation the one with minimal norm (cf. Section 3.3 in Rngl *et al.* [3]) leads to a finite dimensional version

$$s_k^l = \left(T_k^l\right)^* u_k^l \tag{2.12}$$

with

$$A_k^l u_k^l = b_k^l \tag{2.13}$$

of (2.8), where

$$A_k^l := T_k^l \left(T_k^l\right)^*, \quad T_k^l = Q^l T_k, \quad b_k^l := Q^l b_k$$

and Q^l is the orthogonal projection onto Y_l

$$Q^l := Proj_{Y_l}.$$

To find the optimal discretization level according to the discrepancy principle

$$l = \min! \text{ s.t. } \left\|F(v_k) + T_k s_k^l - \Phi^\delta\right\| \leqslant \eta_k \|F(v_k) - \Phi^\delta\|, \tag{2.14}$$

some iterative procedure has to be used, starting at a very coarse level of discretization and successively refining until the linear residual is sufficiently small. Here it would be clumsy to solve the full discrete equation at each refinement level from scratch. Instead, we use the solution obtained on the coarser level as a starting guess for an iterative process

https://doi.org/10.1017/S0956792502005089 Published online by Cambridge University Press

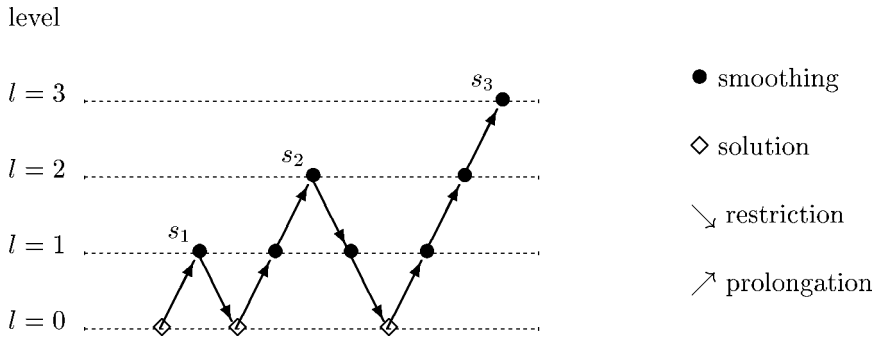


FIGURE 2. The full multigrid method with $q(m) \equiv 1$ and V-cycle multigrid preconditioning.

finding the solution on the next finer level. The direct solution of system (2.13) then only has to be done on the coarsest level. In principle, any iterative regularization method such as Conjugate Gradient (CG) or Landweber could be used for approximately solving the linear system on each finer discretization level; due to the small size of the systems, such a single iteration step does not count in the overall effort as compared to a forward solution. However, the ill-posedness can cause a very slow convergence of this iteration, i.e., a large number of iterations may be necessary to get a reasonable approximation of the Newton step, and thus lead to a considerable contribution to the overall computational effort. Therefore it is advisable to precondition the iteration, which can be done in a very effective way by means of multigrid operators (see the numerical experiments in Subsection 4.1). In this way we arrive at a nested iteration technique (or full multigrid method FMGM, e.g. cf. Hackbusch [6], and, for ill-posed problems, Kaltenbacher [11] and King [15]), which is summarized in the following Algorithm 1, where we leave out the Newton step subscripts k for simplicity of notation.

Algorithm 1

Set $u^0 := (A^0)^{-1}b^0 =: u^0_{(0)}, \quad q(0) := 0$
For $m = 1 \dots l$
  Set $u^m_{(0)} := u^{m-1}_{(q(m-1))}$
  For $i = 1 \dots q(m)$
    Set $u^m_{(i)} = u^m_{(i-1)} + M^m\left(b^m - A^m u^m_{(i-1)}\right)$
Set $s^l := (T^l)^* u^l_{(q(l))}$

where $q(m) \geqslant 1$, and $b^m = Q^m b$. In the simple but most important situation of $q(m) \equiv 1$ and V-cycle multigrid preconditioners M^m, this can be schematically represented as in Figure 2.

If the preconditioners M^m are effective enough to satisfy

$$\|I - (T^m)^* M^m T^m\|_X \leqslant c < 1, \quad \forall m \leqslant l \tag{2.15}$$

https://doi.org/10.1017/S0956792502005089 Published online by Cambridge University Press

with a constant c independent of the refinement level and $q(m) \equiv 1$, or

$$\|I - (T^m)^* M^m T^m\|_X \leqslant c(m) < 1, \quad \forall m \leqslant l$$

with $\frac{1}{1-c(m)}$ growing only moderately with m so that

$$\|(I - (T^m)^* M^m T^m)^{q(m)}\|_X \leqslant c < 1, \quad \forall m \leqslant l$$

holds uniformly with a slowly increasing sequence $q(m)$, we get (cf. e.g. Kaltenbacher [11]) for the difference between s^l and the exact solution $\bar{s}^l = (T^l)^\dagger b^l$ of (2.12), (2.13)

$$\|s^l - \bar{s}^l\|_X \leqslant c^m \frac{1}{1-c} \|\bar{s}^l\| + \frac{1}{\sqrt{1-c^2}} \|(Proj_{(T^m)^* Y_m} - I)\bar{s}^l\|_X,$$

for any $m \leqslant l$, hence, (e.g. with $m := l/2$)

$$\|s^l - \bar{s}^l\|_X \to 0 \quad \text{as } l \to \infty.$$

As shown in Kaltenbacher [11], the number of iterations necessary for reaching an appropriate stopping index (e.g. defined by a discrepancy principle, i.e. l as given by (2.14)) is much smaller than for conventional iterative regularization methods like Landweber or CG. The necessary finest level of discretization for obtaining the required accuracy is theoretically the same. However, it would not be clear at all, how to find it practically if standard CG or Landweber were used. It is mainly for this latter reason that we consider full multigrid as a most effective solution method in our actual context, where it is crucial to keep the data space dimension as small as possible.

Alternatively we can also directly apply a *nonlinear full multigrid method* (see Brandt [1] and Hackbusch [6], for ill-posed problems Kaltenbacher [12]) for the iterative solution of (2.4). This is defined by generalizing the linear case to

Algorithm 2

Set $v_{start} := v^0$
Set $v^0 := SOL(v_{start}, Q^0 \Phi^\delta)$
For $m = 1, \dots l$
    Set $v_{start} := v^{m-1}$
    Set $\tilde{f}^{m-1} := Q^{m-1} F(v^{m-1})$
    Set $v^m := NMGM(k, v_{start}, \tilde{f}^{m-1}, Q^m \Phi^\delta)$

Here $NMGM$ is a nonlinear multigrid operator (see the end of § 2.3) for the projected equation on the mth level

$$Q^m F(v) = Q^m \Phi^\delta, \tag{2.16}$$

starting from $v_{start} \in Y_m$, and SOL is an approximation method – usually just Newton's method – for the solution of (2.16) on the coarsest level $m = 0$. It can be shown in a general framework of nonlinear ill-posed operator equations (2.7), that under certain conditions, this iterative procedure equipped with a stopping rule of discrepancy type defines a regularization method for the underlying infinite-dimensional operator equation, i.e. $v^{l(\delta)} \to v$ as $\delta \to 0$.

https://doi.org/10.1017/S0956792502005089 Published online by Cambridge University Press

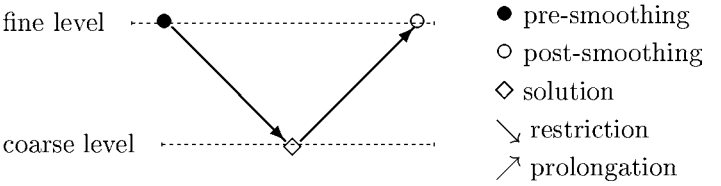


FIGURE 3. Two grid method.

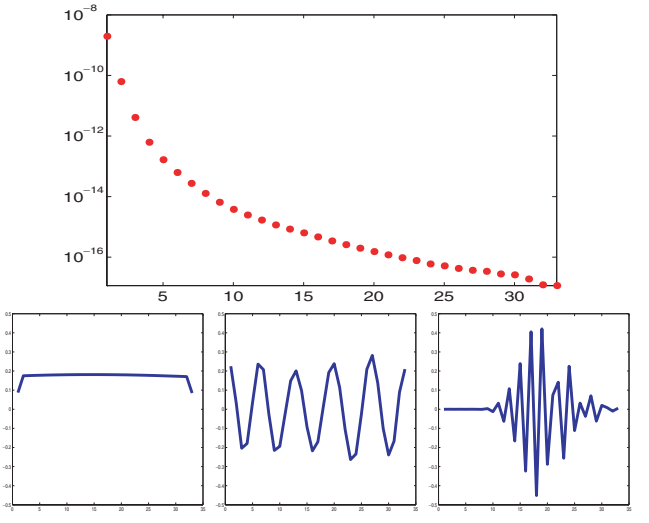


FIGURE 4. Singular values as well as 1st, 11th and 33rd eigenfunction of T_k.

2.3 Multigrid methods for ill-posed problems

Multigrid operators, although well-known to be extremely efficient tools for well-posed problems such as elliptic Partial Differential Equations (PDEs) or second kind integral equations (e.g. cf. Hackbusch [6]), have until recently not been so well understood in the context of ill-posed problems. The reason for the difficulties lies in the proper construction of smoothing operators. To make this point clear we recall the definition of multigrid operators by means of the most simple two-grid case (see Figure 3). Usually, the smoothing operators are defined by, for example, Jacobi, Gauss-Seidel, or SOR iterations which in the case of standard elliptic PDEs damp out the high frequency components of the defect on the finer grid to make it well representable on the coarser grid. In ill-posed problems, these methods lose their smoothing properties, due to the fact that small eigenvalues of compact operators correspond to high frequency eigenvalues, e.g. see Figure 4 for the first 33 eigenvalues and three of the corresponding eigenfunctions in case of the operator T_k given by the linearization of our *B–H* curve identification problem.

An idea for constructing smoothers for general linear ill-posed problems

$$Ts = b,$$

https://doi.org/10.1017/S0956792502005089 Published online by Cambridge University Press

originating from a paper by King [15] and further investigated in Kaltenbacher [11, 12], is based on subspace decomposition. By seperating the high from the low frequency parts within some actual discretization space Y_l by simple projection, and amplifying the high frequencies with an appropriate factor ξ_l, while just removing the low frequencies, the operator

$$S^l := \xi_l [I - Q^{l-1}] Q^l \tag{2.17}$$

with

$$\xi_l \sim h_l^{-2p},$$

can indeed be shown to decrease the high frequency part in the defect to such an extent, that the rest can be well enough approximated on the coarser level. Here h_l is the mesh size on the lth level and p the degree of ill-posedness (here $p = \frac{3}{2}$ – see Proposition 1). This motivates the definition of multigrid operators M^l in the usual recursive way:

Algorithm 3

Set $M^0 := (A^0)^{-1}$
Assume that M^{l-1} *has been defined and define* M^l *for* $b^l \in Y_l$ *as follows:*

Set $u := 0$
Set $u := u + S^l(b^l - A^l u)$ (pre-smoothing)
Set $s := 0$
For $i = 1 \ldots \gamma(l)$
Set $s := s + M^{l-1}(Q^{l-1}(b^l - A^l u) - A^{l-1} s)$
Set $u := u + s$. } (coarse grid correction)
Set $u := u + S^l(b^l - A^l u)$ (post-smoothing)
Set $M^l b^l := u$.

where $A^l := Q^l T (Q^l T)^*$, $b^l = Q^l b$, and $\gamma(l) \geqslant 1$ describes the cycle regime: $\gamma(l) \equiv 1$ corresponds to the V-cycle, $\gamma(l) \equiv 2$ to the W-cycle and $\gamma(l) = 2 - \mathrm{mod}(l, 2)$ to the alternating cycle. For the so defined multigrid operators it can be shown (using basically the smoothing property of the forward operator T and the approximation property of the spaces Y_l), that it satisfies the preconditioning criterion (2.15) with a level independent constant c, if one uses W- or alternating MG cycles (cf. Kaltenbacher [11]). If one applies more sophisticated smoothers, one can even show V-cycle convergence with level independent contraction factor c in 2.15 – see Kaltenbacher [13]. Analogous results can be obtained for the additive multigrid operators

$$M^l = \sum_{m=1}^{l} \xi_m [I - Q^{m-1}] Q^m + Q^0. \tag{2.18}$$

Here it also becomes clear why we set $\xi_l \sim h_l^{-2p}$: the resulting MG operator (2.18) represents a discrete differential operator of order $2p$ and is in this sense an approximate inverse of the discrete version A^l of TT^*, so that it can be expected to serve as a good preconditioner. As a consequence, we can apply the assembled operators M^l as

https://doi.org/10.1017/S0956792502005089 Published online by Cambridge University Press

preconditioners in the full multigrid Algorithm 1 for the regularized solution of the Newton step equation (2.8) in our B–H curve identification procedure and expect to obtain the convergence behaviour as indicated in the previous section.

In the alternative inversion approach based on a nonlinear full multigrid method (see Algorithm 2), we need nonlinear multigrid operators. These can be defined by generalizing the multigrid recursion as well as the smoothing operators according to Algorithm 4:

Algorithm 4

Set $NMGM(0, v_{start}, \tilde{f}^{-1}, f^0) := SOL(v_{start}, f^0)$.
Assume that $NMGM(l-1,\cdot,\cdot,\cdot)$ *and* v^{l-1} *have been defined and define* $NMGM(l, v_{start}, \tilde{f}^{l-1}, f^l)$ *for* $\tilde{f}^{l-1} \in Y_{l-1}$ $f^l \in Y_l$ *as follows:*

Set $v := S^l(v_{start}, f^l)$
Set $d^{l-1} := Q^{l-1}(F(v) - f^l)$
Choose $\lambda \in \mathbb{R}^+$
Set $d^{l-1} := \tilde{f}^{l-1} - \lambda d^{l-1}$
Set $s^{l-1} := v^{l-1}$
For $i = 1, \ldots \gamma(l)$
  Set $s^{l-1} = NMGM(l-1, s^{l-1}, \tilde{f}^{l-1}, d^{n-1})$
Set $v = v + \frac{1}{\lambda}(s^{l-1} - v^{l-1})$
Set $NMGM(l, v_{start}, \tilde{f}^{l-1}, f^l) := v$

where

$$S^l(v_{start}, f^l) = v_{start} - \xi_l T_k^* [I - Q^{l-1}](Q^l F(v_{start}) - f^l),$$

(see Kaltenbacher [12], where the choice of the relaxation parameter λ is also discussed).

3 Some realization aspects

3.1 Measurement Setup

To collect the data we propose an experimental setup sketched in Figure 5. Here, a DC (directed current) source provides the prescribed excitation current at an actual measurement point I, which has to be in a high amplitude range in order to reach the nonlinear part of the B–H curve. This is superimposed on an alternating current of very small amplitude (so that it can be neglected in the numerical simulations) in order to enable measurements of the inductance L via a Wheatstone bridge. From the relation

$$L = n_w \frac{\Phi}{I}$$

where n_w is the number of coil windings, we then get the value of the flux Φ corresponding to I. This is done repeatedly for different values of I in order to obtain a collection of points along the I–Φ curve.

https://doi.org/10.1017/S0956792502005089 Published online by Cambridge University Press

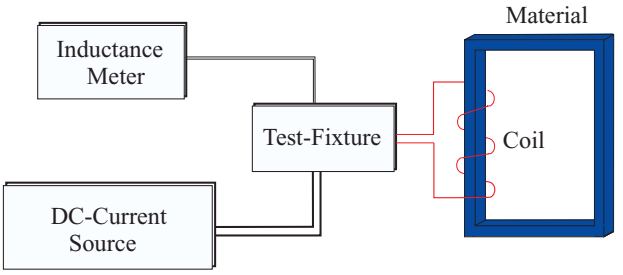


FIGURE 5. Measurement setup.

3.2 Numerical solution of the forward problems

The forward evaluation that is necessary to determine the data misfit for a given parameter configuration as it has to be done repeatedly during the inversion iteration, consists in the numerical solution of the nonlinear vectorial three-dimensional BVPs (1.3). By locally linearizing iterations, i.e. solution of the nonlinear field problem (1.3) by a Newton type method, we arrive at a sequence of linear boundary value problems, whose variational formulation reads as: For all $I \in \{I_1, \ldots, I_{d(n)}\}$ find $\mathbf{S}^I \in H_0(curl)$ such that, for all $\mathbf{A}' \in H_0(curl)$:

$$\begin{aligned} &\int_D \nabla \times \mathbf{A}' \cdot \left(\nu(B^I) + \nu'(B^I) B^I proj_{\mathbf{e}_{B^I}}\right), \nabla \times \mathbf{S}^I \; dV \\ &\quad = I \frac{1}{|\Omega_c|} \int_{D_c} \mathbf{A}' \cdot \mathbf{e}_J \; dV - \int_D \nabla \times \mathbf{A}' \cdot \nu(B^I) \mathbf{B}^I \; dV, \end{aligned} \tag{3.1}$$

where

$$\mathbf{B}^I = \nabla \times \mathbf{A}^I, \quad B^I = |\mathbf{B}^I|, \quad \mathbf{e}_{B^I} = \frac{1}{B^I} \mathbf{B}^I, \quad proj_{\mathbf{e}_{B^I}} := \mathbf{e}_{B^I} \mathbf{e}_{B^I}^T,$$

and $\{I_1, \ldots, I_{d(n)}\}$ is the set of measurement points actually taken into account according to the discretization strategy described in the previous section.

The Finite Element (FE) method with edge or nodal elements

$$\mathbf{A}^I \approx \sum_k A_k \mathbf{N}_k$$

leads to a large discrete system

$$\mathbf{K}_h \{A_h\} = \{J_h\}$$

which is solved in a most efficient way by CG iterations with algebraic or geometric multigrid preconditioners – for details we refer to Kaltenbacher *et al.* [14]. To give a feeling of the numerical performance of our forward solver, we provide a few results on computational times for the linearized forward problem (see Table 1) and for the nonlinear forward problem, when solved by Newton's method (see Table 2) for several levels of discretization. Here, the discretization was done with nodal finite elements and an algebraic multigrid solver was used to precondition the conjugate gradient iteration. In these tests, the prescribed accuracy was 10^{-6} for the energy norm of the error in the PCG

https://doi.org/10.1017/S0956792502005089 Published online by Cambridge University Press

Table 1

No. of unknowns	PCG iterations	CPU time (sec.)
8244	17	4
29694	24	21.6
72219	40	76

Table 2

No. of unknowns	Newton iterations	CPU time(sec.)
8244	7	29
29694	5	111
72219	8	604

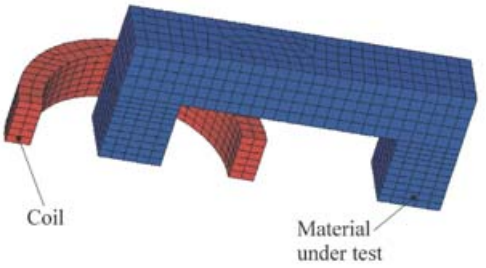


FIGURE 6. Computational mesh (partial).

iterations and 10^{-2} for the relative residual in the Newton iteration. The computations were done on an SGI Octane 300 mHz. See Figure 6 for part of the computational grid used; the actual computational domain covers the material, the coil, as well as the surrounding air region, using the symmetry along the horizontal cross-sectional plane.

To save computational effort, the Newton iteration for approximating a solution $\mathbf{A}^I$ of (2.1) is stopped as soon as an accuracy sufficient for our inversion procedure is attained. At the beginning of the inversion iteration, i.e. 'far away' from the solution, we require a lower level of precision than at a converged state. More precisely, it is sufficient to do an approximate evaluation $\tilde{F}(v_k)$ such that

$$\|\tilde{F}(v_k) - F(v_k)\| \leqslant c\|\tilde{f}(v_k) - \Phi^\delta\| \tag{3.2}$$

for some constant $c < 1$. From the fact that the difference $\mathbf{D}_A^I = \tilde{\mathbf{A}}^I - \mathbf{A}^I$ between an approximate solution $\tilde{\mathbf{A}}^I$ and the exact one $\mathbf{A}^I$ of (2.1) satisfies

$$\int_D \nabla \times \mathbf{A}' \cdot \overline{\nu}\, \nabla \times \mathbf{D}_A^I \, dV \;=\; res^I[\mathbf{A}'] \quad \forall \mathbf{A}' \in H_0(curl),$$

https://doi.org/10.1017/S0956792502005089 Published online by Cambridge University Press

with

$$res^I[\mathbf{A}'] := \int_D \nabla \times \mathbf{A}' \cdot \nu(|\nabla \times \tilde{\mathbf{A}}^I|)\, \nabla \times \tilde{\mathbf{A}}^I \; dV - I \frac{1}{|\Omega_c|} \int_{D_c} \mathbf{A}' \cdot \mathbf{e}_J \; dV$$

and $\overline{\nu} = \nu_k(\tilde{B}) + \int_0^1 (\nu_k'(B + \theta(\tilde{B} - B))\, d\theta$ (which is bounded away from zero and sufficiently smooth), we can conclude

$$\begin{aligned} \|\tilde{F}(\nu_k) - F(\nu_k)\|_Y^2 &\leqslant C \int_{[\underline{I},\overline{I}]} \|\nabla \times \mathbf{D}_A^I \cdot \mathbf{n}\|^2_{L^2(\Omega_c)} \; dI \\ &\leqslant C \int_{[\underline{I},\overline{I}]} \|\nabla \times \mathbf{D}_A^I\|^2_{L^2(\Omega_c \times [0,h])} \; dI \leqslant C \int_{[\underline{I},\overline{I}]} \|res^I\|^2_{L^2(D)} \; dI, \end{aligned}$$

where we have used the averaging flux evaluation (2.3) in the second inequality. Therefore, we can guarantee (3.2) by making the $L^2([\underline{I},\overline{I}])$ norm of the residuals $\|res^I\|_{L^2(D)}$ smaller than the computable quantity $\|\tilde{f}(\nu_k) - \Phi^\delta\|$, multiplied with some sufficiently small but fixed factor c.

3.3 Curve approximation

As can be seen from (2.9), (3.1) above, not only values but also first derivatives of ν are required for the forward simulation. Since on one hand we have to be able to evaluate ν at any point attained by B, and on the other hand can only do computations with discrete quantities, we use spline representations for both functions ν and ν'. During the inversion iteration these are obtained by appropriate updating the splines ν and ν'. A crucial point is to obtain good starting functions $B \to \nu_0(B), B \to \nu_0'(B)$. Via the formulas (1.2) we get, from our measurements of the I–Φ curve, points $(B^i, H^i)_{i=1\ldots d(I)}$ defining a plausible starting curve $\nu_0 = H/B$. Since we want to get an initial guess also for the derviative, the assingment of a spline to this collection of points is a nontrivial task and ill-posed (just like the B–H curve identification problem itself as discussed for the case of uniform magnetic field in Section 2.1), since it involves numerical differentiation of the data: Note that we want to reconstruct first derivatives from pointwise value measurements. This is done in a stabilized way by using so-called smoothing splines (cf. [2]) or, in other words minimizing a regularized least squares functional

$$J^\alpha[B] = \alpha \|B''\|^2_{L^2} + \sum_{i=1}^{d(I)} (B(H^i) - B^i)^2$$

over the set of third order C^1 Hermite splines $B : H \to B(H)$. For determining the reguarization parameter α a posteriori, we use a discrepancy principle with bisection, i.e. set α equal to the largest member of the geometrically decreasing sequence 2^{-j} such that for the minimizer B^α of J^α the residual $\sum_{i=1}^{d(I)} (B(H^i) - B^i)^2$ is of the order of magnitude of the measurement noise; see Figure 7 for an example of such a curve approximation and its derivative with one per cent noise. Note that – unlike ν – the B–H curve itself always has to be monotone for physical reasons, so to be able to monitor and preserve this property, we do not precompute points $(\nu^i, B^i) = (\frac{H^i}{B^i}, B^i)$ and do the smoothing spline approximation for those, but prefer to apply the described smoothing spline technique directly to the collection of (B^i, H^i) points (from which we get, by $\nu_0 = \frac{H_0}{B}$, $\nu_0' = \frac{H_0' B - H_0}{B^2}$

https://doi.org/10.1017/S0956792502005089 Published online by Cambridge University Press

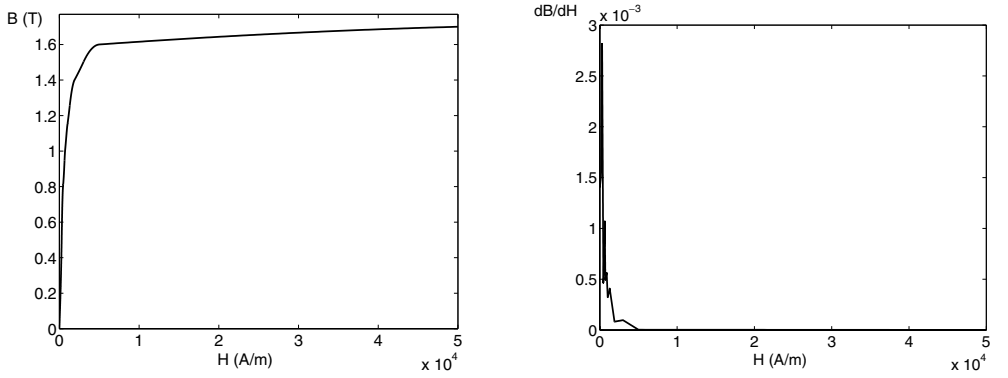


FIGURE 7. Approximation of function values and derivatives from pointwise measurements by smoothing splines.

points on the curves v_0, v_0', whose C^1 interpolation yields the splines used in the initial step of our computations). Practically, the monotonicity of the B–H curve approximation is gained by putting restrictions on the coefficients of the spline curve. These restrictions arise naturally, if we require $B'(H) > 0$. Consequently, the task is to find a monotone approximation, which fulfils the discrepancy principle for a given data noise level. Note, additionally, that the noise level is given in terms of the I–$\Phi(I)$ values and therewith for the (H^i, B^i) points. If we would deduce an estimate for the data noise in terms of the (v^i, B^i) points, this would, due to the strong variation in scale of both function and derivative values of the curve under consideration, lead to a locally too pessimistic noise estimate, and hence to a bad curve approximation.

We mention that this smoothing spline technique itself can be considered as a stable solution method for the ill-posed problem of B–H curve identification in the special situation of uniform magnetic field.

4 Numerical results

4.1 Tests of multigrid operators for T_k

First of all we do some numerical experiments to test the behavior of multigrid operators as described in § 2.3 for the linearized parameter identification problems (2.8).

Figure 8 is intended to demonstrate the main difference between multigrid methods with a conventional smoothing operator and with the one given in § 2.3. While with a point Gauss-Seidel smoother the Preconditioned Conjugate Gradient (PCG) method stalls after a few iterations (by the way a phenomenon which has also been observed for other ill-posed problems –cf. Henson *et al.* [7] for an inverse problem from computerized tomography), the smoother according to (2.17) preserves a good convergence rate.

To illustrate the preconditioning quality of the proposed multigrid operators, we directly compare the condition numbers of the operators A^l (that strongly grow due to ill-posedness) to that of the multigrid preconditioned operators, that exhibit a significant improvement (see Figure 9).

https://doi.org/10.1017/S0956792502005089 Published online by Cambridge University Press

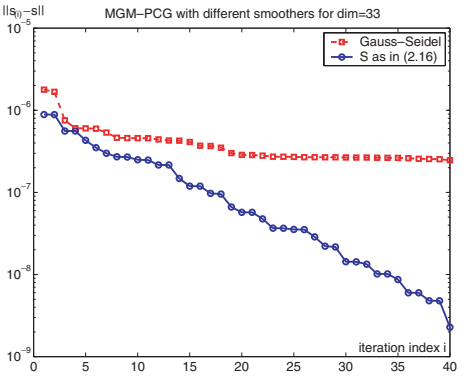


FIGURE 8. Conjugate gradient convergence with multigrid preconditioning using conventional smoother versus (2.17).

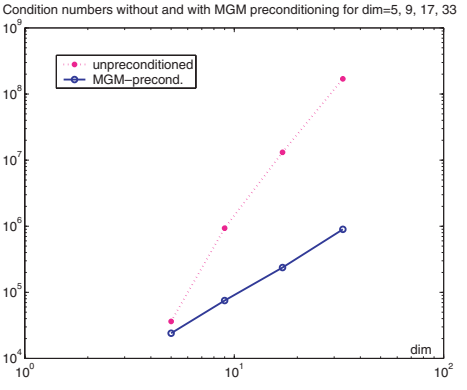


FIGURE 9. Condition numbers without and with appropriate multigrid preconditioning.

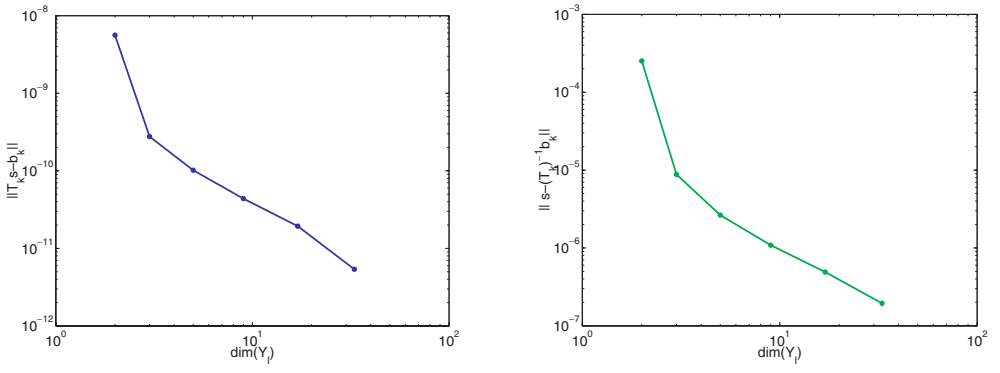


FIGURE 10. Convergence of the full multigrid method for $T_k s = b_k$.

https://doi.org/10.1017/S0956792502005089 Published online by Cambridge University Press

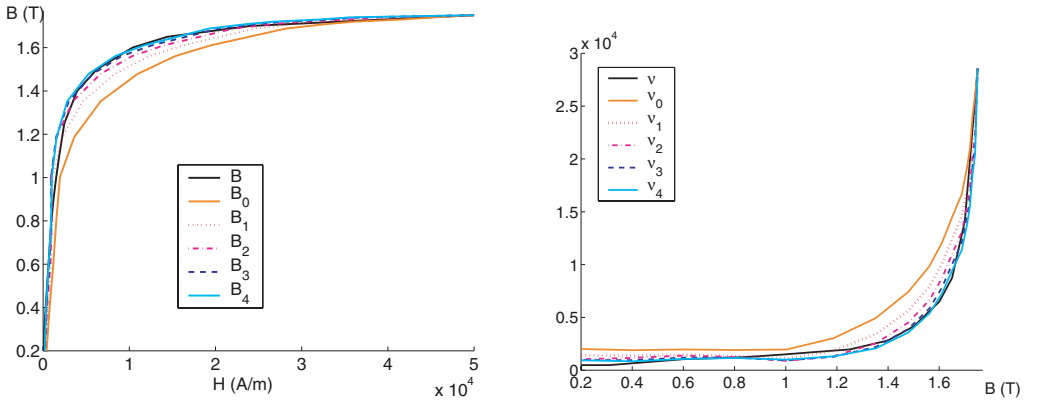


FIGURE 11. Convergence with exact data: H–B curves (left) and B–ν curves (right).

In Figure 10, convergence of the full multigrid method is demonstrated. Both the residual and the error in pre-image space show the expected good convergence behaviour. Note that we have implemented V-cycle multigrid operators with only one iteration per level ($q(m) \equiv 1$), so that already the computationally cheapest version of FMGM is satisfactory. As a right-hand side we here chose the same as for our PCG tests shown in Figure 8.

4.2 B–H curve reconstructions

First we do some computations with exact data. Figure 11 shows the starting curve and the first six Newton iterates (using FMGM to approximate the Newton step) compared to the exact curve. The finest discretization level corresponds to 17 measurement points.

To do tests with noisy data, we generate synthetic data corresponding to the prescribed exact curve by forward computations on a finer FE mesh and adding random noise of the respective noise level (thus avoiding an 'inverse crime'). Figures 12, 13 and 14 show the first four Newton iterates with 1%, 2% and 3% noise, respectively. Note that in a realistic experimental setup, the measurement noise is between 1% and 2% at most.

Here the finest discretization level according to the rule (2.14) is only used in the last step according to (2.10) (i.e. the second step in case $\delta = 2\%$ or 3% and the third step in case $\delta = 1\%$,) so that the effort can be reduced to 60% in case $\delta = 2\%, 3\%$ and even to 50% in case $\delta = 1\%$, as compared to a full discretization in each Newton step.

A more precise look at the iteration error by plotting the relative error of the B–ν curves (see Figure 15) shows that indeed, due to the ill posedness, the iterates following the ones chosen according to (2.10) would have become worse again, and therefore confirms that (2.10) is an appropriate stopping criterion for the Newton inversion iteration.

In a second test series we consider a B–H curve whose curvature changes sign close to the origin, as it is typical for some materials. In Figure 16 the obtained overall reconstructions from data with 1% noise are shown. Figure 17 views the details in the first part of the curves which makes obvious, that the curvature change, that is not visible

https://doi.org/10.1017/S0956792502005089 Published online by Cambridge University Press

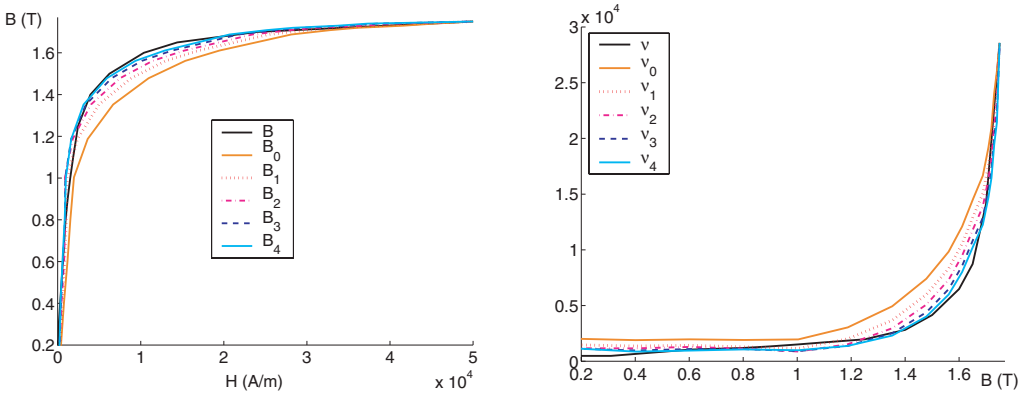


FIGURE 12. Convergence with noisy data ($\delta = 1\%$ noise): H–B curves (left) and B–ν curves (right).

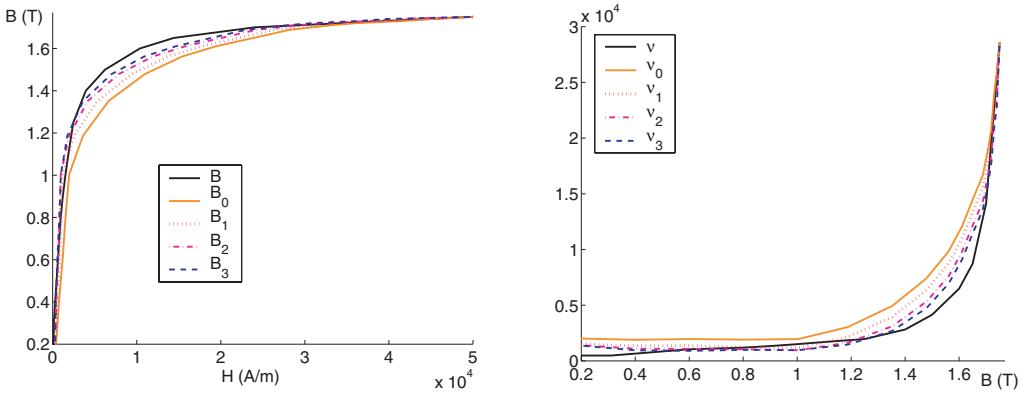


FIGURE 13. Convergence with noisy data ($\delta = 2\%$ noise): H–B curves (left) and B–ν curves (right).

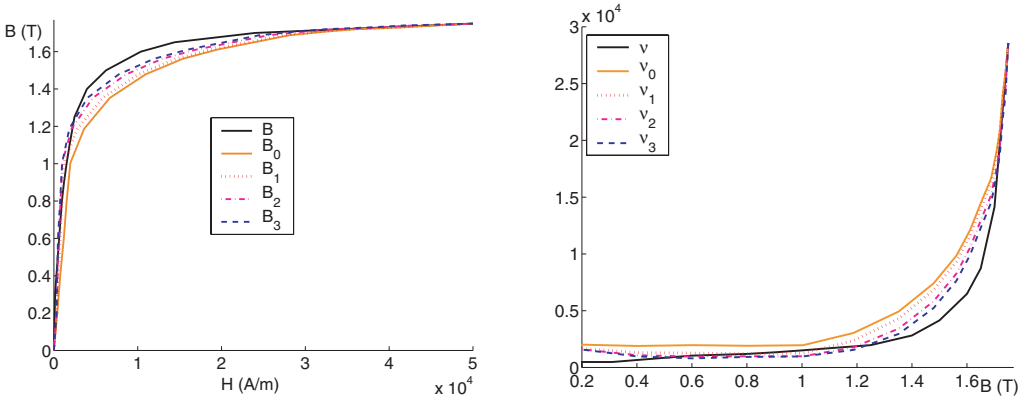


FIGURE 14. Convergence with noisy data ($\delta = 3\%$ noise): H–B curves (left) and B–ν curves (right).

https://doi.org/10.1017/S0956792502005089 Published online by Cambridge University Press

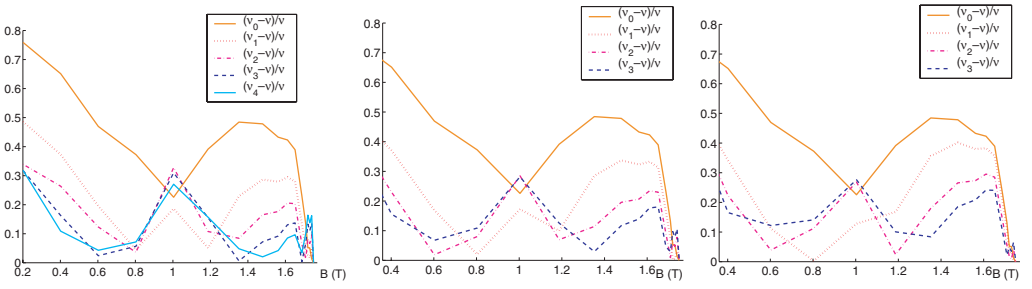


FIGURE 15. Relative error $B \to \frac{\nu_i(B)-\nu(B)}{\nu(B)}$ for 1%, 2% and 3% noise.

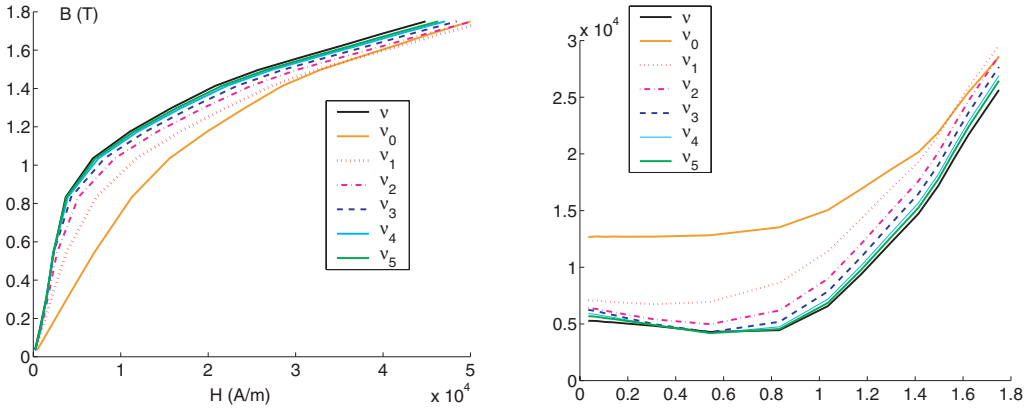


FIGURE 16. Second example: Convergence with noisy data ($\delta = 1$ % noise): H–B curves (left) and B–ν curves (right).

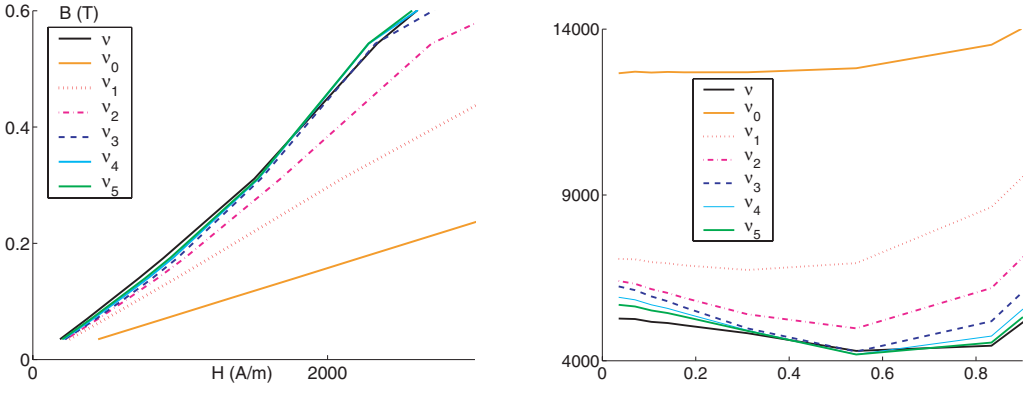


FIGURE 17. Second example: Detailed view of curvature change: H–B curves (left) and B–ν curves (right).

https://doi.org/10.1017/S0956792502005089 Published online by Cambridge University Press

from the data (i.e. the I–Φ curve that we used at our starting guess) is well reproduced by the inversion algorithm.

5 Conclusions and remarks

In the context of magnetism with large excitation amplitudes we often will not only encounter nonlinearity, but also hysteresis effects. Note that the identification of hysteresis curves is possible in a principally similar way to our proposed reconstruction scheme of B–H curves as real functions. For instance, the identification of a Preisach model can be seen as the reconstruction of function of two variables (the weight function) and two constants (the polarization values).

The proposed method is also applicable to several other parameter identification problems or even to other inverse problems. Note that the inversion principles presented here are quite general.

A parameter identification problem that is in many aspects similar to the one considered here, is the reconstruction of the material tensors $\mathbf{c}^E = \mathbf{c}^E(|\mathrm{DIV}^T\mathbf{d}|, |\mathrm{grad}\ \phi|)$, $\mathbf{e} = \mathbf{e}(|\mathrm{DIV}^T\mathbf{d}|, |\mathrm{grad}\ \phi|)$, $\varepsilon^S = \varepsilon^S(|\mathrm{DIV}^T\mathbf{d}|, |\mathrm{grad}\ \phi|)$ of nonlinear piezoelectric media in

$$\begin{aligned} \rho\omega^2\mathbf{d} + \mathrm{DIV}(\mathbf{c}^E\mathrm{DIV}^T\mathbf{d} + \mathbf{e}^T\mathrm{grad}\ \phi) = 0 \quad & \text{in } \Omega \\ -\nabla(\mathbf{e}\mathrm{DIV}^T\mathbf{d} - \varepsilon^S\mathrm{grad}\ \phi) = 0 \quad & \text{in } \Omega, \end{aligned} \tag{5.1}$$

from electrical and mechanical measurements for different frequencies ω. Here, $\mathbf{d} = (d_x, d_y, d_z)$ are the mechanical displacements, ϕ the electric potential, ρ the density, ω the frequency, and DIV denotes the divergence of a dyadic. Analogies to the B–H curve identification problem in magnetics are:

- One forward problem consists of solving several BVPs namely (5.1) for different frequencies ω.
- The searched for parameter depends nonlinearly on the field quantities, more precisely on first derivatives of the state variables.
- The differential operator is of second order wrt. the state variable and of first order wrt. the searched for parameter.
- Hysteresis effects may appear.

The piezoelectric parameter identification problem has to be expected to be more complicated, though: more parameters and more field quantities are involved and the underlying system of PDEs is indefinite instead of elliptic.

Acknowledgement

The authors wish to thank Dr. Michael Kuhn for interesting discussions on theoretical and numerical aspacts of magnetic field computation. Moreover we acknowledge fruitful remarks by the referees on a first version of this paper.

Support by the Fonds zur Förderung der wissenschaftlichen Forschung under grant T 7-TEC and project F1306 within Spezialforschungsbereich F013 is gratefully acknowledged.

https://doi.org/10.1017/S0956792502005089 Published online by Cambridge University Press

Appendix

Proof (Proposition 1)
Fix $\sigma \in (1, \frac{3}{2})$. For any $z \in L^2([\underline{I},\overline{I}])$ we have

$$\begin{aligned}
\|T_k^* z\|_{H^2([\underline{B},\overline{B}])} &= \int_{\mathbb{R}} (1+\xi^2)^2 \left| \int_{[\underline{I},\overline{I}]} z(I) \int_D e^{-iB_k^I \xi} (\mathscr{F}\eta)(\xi) \mathbf{B}_k^I \cdot (\nabla \times \mathbf{Z}^I)\, dV\, dI \right|^2 d\xi \\
&= \int_{\mathbb{R}} \left| \int_{[\underline{I},\overline{I}]} z(I) \int_D e^{-iB_k^I \xi} \frac{1}{1+\xi^2} \mathbf{B}_k^I \cdot (\nabla \times \mathbf{Z}^I)\, dV\, dI \right|^2 d\xi \\
&\leqslant \|z\|_{(H^\sigma([\underline{I},\overline{I}]))^*} \int_{\mathbb{R}} \left(\int_{[\underline{I},\overline{I}]} \left(|\mathbf{W}^{\mathbf{I}}|^2 + \left| \frac{d}{dI} \mathbf{W}^{\mathbf{I}} \right|^2 \right) dI \right)^{2-\sigma} \\
&\qquad \left(\int_{[\underline{I},\overline{I}]} \left(|\mathbf{W}^{\mathbf{I}}|^2 + \left| \frac{d}{dI} \mathbf{W}^{\mathbf{I}} \right|^2 + \left| \frac{d^2}{dI^2} \mathbf{W}^{\mathbf{I}} \right|^2 \right) dI \right)^{\sigma-1} d\xi
\end{aligned} \tag{5.1}$$

where

$$W^I := \int_D e^{-iB_k^I \xi} \frac{1}{1+\xi^2} \mathbf{B}_k^I \cdot (\nabla \times \mathbf{Z}^I)\, dV$$

and we have used the interpolation inequality

$$\forall w \in H^2([\underline{I},\overline{I}]) \quad : \quad \|w\|_{H^\sigma([\underline{I},\overline{I}])} \leqslant \|w\|^{2-\sigma}_{H^1([\underline{I},\overline{I}])} \|w\|^{\sigma-1}_{H^2([\underline{I},\overline{I}])}.$$

The derivatives of W^I with respect to I are

$$\begin{aligned}
\frac{d}{dI}\mathbf{W}^{\mathbf{I}} = \int_D e^{-iB_k^I \xi} \Bigg(& \frac{-i\mathbf{e}_{B_k^I} \cdot \mathbf{B}_{k\ I}^I \xi}{1+\xi^2} \mathbf{B}_k^I \cdot (\nabla \times \mathbf{Z}^I) \\
& + \frac{1}{1+\xi^2} \left(\mathbf{B}_{k\ I}^I \cdot (\nabla \times \mathbf{Z}^I) + \mathbf{B}_k^I \cdot \left(\nabla \times \mathbf{Z}_I^I\right) \right) \Bigg) dV
\end{aligned}$$

$$\begin{aligned}
\frac{d^2}{dI^2}\mathbf{W}^{\mathbf{I}} = \int_D e^{-iB_k^I \xi} \Bigg(& \frac{-\left(\mathbf{e}_{B_k^I} \cdot \mathbf{B}_{k\ I}^I\right)^2 \xi^2}{1+\xi^2} \mathbf{B}_k^I \cdot (\nabla \times \mathbf{Z}^I) \\
& + \frac{-i\left(\mathbf{e}_{B_k^I} \cdot \mathbf{B}_{k\ II}^I - \left|\left(id - proj_{\mathbf{e}_{B_k^I}}\right) \mathbf{B}_{k\ I}^I\right|^2 / B_k^I\right) \xi}{1+\xi^2} \mathbf{B}_k^I \cdot (\nabla \times \mathbf{Z}^I) \\
& + 2\frac{-i\mathbf{e}_{B_k^I} \cdot \mathbf{B}_{k\ I}^I \xi}{1+\xi^2} \left(\mathbf{B}_{k\ I}^I \cdot (\nabla \times \mathbf{Z}^I) + \mathbf{B}_k^I \cdot \left(\nabla \times \mathbf{Z}_I^I\right) \right) \\
& + \frac{1}{1+\xi^2} \left(\mathbf{B}_{k\ II}^I \cdot (\nabla \times \mathbf{Z}^I) + \mathbf{B}_k^I \cdot \left(\nabla \times \mathbf{Z}_{II}^I\right) + 2\mathbf{B}_{k\ I}^I \cdot \left(\nabla \times \mathbf{Z}_I^I\right) \right) \Bigg) dV
\end{aligned}$$

with

$$\mathbf{B}_{k\ I}^I := \frac{d}{dI}\mathbf{B}_k^I, \quad \mathbf{B}_{k\ II}^I := \frac{d^2}{dI^2}\mathbf{B}_k^I, \quad \mathbf{Z}_I^I := \frac{d}{dI}\mathbf{Z}^I, \quad \mathbf{Z}_{II}^I := \frac{d^2}{dI^2}\mathbf{Z}^I,$$

https://doi.org/10.1017/S0956792502005089 Published online by Cambridge University Press

so that, by our assumptions, we can further continue our estimate in the last line of (5.1) according to

$$\|T_k^* z\|_{H^2([\underline{B},\overline{B}])} \leqslant C\|z\|_{(H^\sigma([\underline{I},\overline{I}]))^*} \int_{\mathbb{R}} \left(\frac{1}{1+\xi^2}\right)^{2-\sigma} d\xi,$$

where the integral over $\mathbb{R}$ is finite as long as $2(2-\sigma) > 1$, i.e., $\sigma < \frac{3}{2}$. Since $L^2([\underline{I},\overline{I}])$ is dense in $(H^\sigma([\underline{I},\overline{I}]))^*$, the assertion follows. □

References

[1] Brandt, A. (1977) Multilevel adaptive solutions to boundary value problems. *Math. Comp.* **31**, 333–390.
[2] de Boor, C. (1978) *A Practical Guide to Splines*. Springer.
[3] Engl, H. W., Hanke, M. & Neubauer, A. (1996) *Regularization of Inverse Problems*, Kluwer.
[4] Evans, L. C. (1998) *Partial Differential Equations*. AMS.
[5] Groetsch, C. W. (1993) *Inverse Problems in Mathematical Sciences*. Vieweg, Braunschweig.
[6] Hackbusch, W. (1985) *Multi-grid Methods and Applications*. Springer.
[7] Henson, V. E., Limber, M. A., McCormick, S. F. & Robinson, B. T. (1996) Multilevel image reconstruction with natural pixels. *SIAM J. Sci. Comp.* **17**, 193–216.
[8] Ida, N. & Bastos, J. P. (1992) *Electromagnetics and calculation of fields*. Springer.
[9] Ioan, D., Rebican, M. & Gasparics, A. (1999) *B–H* characteristic extraction using devices with non-uniform magnetic field. *COMPEL 18*, pp. 469–482.
[10] Kaltenbacher, B. (2000) Regularization by projection with a posteriori discretization level choice for linear and nonlinear ill-posed problems. *Inverse Problems*, **16**, 1523–1539.
[11] Kaltenbacher, B. (2001) On the regularizing properties of a full multigrid method for ill-posed problems. *Inverse Problems*, **17**.
[12] Kaltenbacher, B. (2000) A multi-grid method with a priori and a posteriori level choice for the regularization of nonlinear ill-posed problems. SFB013-report No.00-3, University of Linz.
[13] Kaltenbacher, B. (2000) V-cycle convergence of some multigrid methods for ill-posed problems. SFB013-report, University of Linz.
[14] Kaltenbacher, M., Reitzinger, S., Schinnerl, M., Schöberl, J. & Landes, H. (2001) Multigrid methods for the computation of 3D electromagnetic field problems. *COMPEL 20*.
[15] King, J. T. (1992) Multilevel algorithms for ill-posed problems. *Numer. Math.* **61**, 311–334.
[16] Louis, A. K. (1989) *Inverse und schlecht gestellte Probleme*. Teubner.
[17] Morozov, V. A. (1993) *Regularization Methods for Ill-posed Problems*. CRC Press.
[18] Natterer, F. (1986) *The Mathematics of Computerized Tomography*. Teubner,
[19] Tikhonov, T. N. & Arsenin, V. A. (1979) *Methods for Solving Ill-posed Problems*. Nauka, Moscow.
[20] Vainikko, G. M. & Veterennikov, A. Y. (1986) *Iteration Procedures in Ill-posed Problems*. Nauka, Moscow.

https://doi.org/10.1017/S0956792502005089 Published online by Cambridge University Press